LAWRENCE
LIVERMORE
NATIONAL
LABORATORY

LLNL-PROC-656539

Investigation of the Effects of Microstructure and Binder Properties on Impact-Induced Fragmentation in Explosives with Meso-Scale Simulations

B. W. White, H. K. Springer, C. M. May

July 3, 2014

15th International Detonation Symposium
San Francisco, CA, United States
July 13, 2014 through July 18, 2014

Disclaimer

Investigation of the effects of microstructure and binder properties on impact-induced fragmentation in explosives with meso-scale simulations

Bradley W. White[†], H. Keo Springer[†] and Chadd M. May[†]

[†]Lawrence Livermore National Laboratory, 7000 East Avenue, Livermore, CA, 94550, U.S.A.

Abstract. A critical mechanism in delayed XDT (X for unknown Detonation Transition) modes is the fragmentation of energetic materials under high-speed impact loading. Fragment size and spacing distribution, in turn, influence the recompaction initiation and subsequent detonation propagation during XDT. We perform meso-scale simulations to examine the effects of microstructure and binder properties on impact-induced fragmentation behavior. Such studies provide a numerical framework for understanding structure-property relationships and designing new energetic materials with optimized safety properties. We employ a multi-physics arbitrary-lagrangian-eulerian code, ALE3D [1] , for these simulations. Unreacted equation-of-state properties, as well as strength properties, were taken from previous meso-scale studies on HMX. In these simulations the binder strength is varied to reflect the strength of commonly used energetic material binders (e.g., HTPB, Kel-F, PTFE, Epoxy, and Estane). HMX grain size distribution and volume fraction, and binder thickness are also varied to explore microstructural effects.

Introduction

Propellants and explosives that have experienced high velocity insults, such as from bullet or fragment impacts, can undergo reactions that exhibit a delayed transition to detonation [2]. The associated impact stresses are lower and the time to detonation (as much as 100+ microseconds) is much longer than durations observed in the shock-to-detonations (SDT), which occur approximately within the first passing shock front (few microseconds). This type of detonation transition is referred to as an unknown-to-detonation transition (XDT) since the mechanisms that lead up to detonation are not entirely known. The common thought however, is that XDT reactions modes are a result of increased sensitivity following a propagating pressure front due to damage nucleation in the form of porosity and cracks. In burn-to-violent reaction (BVR) experiments [3] and XDT experiments [4, 5] the recompaction of damaged propellants is considered an initiation mode that leads to detonation, as are friction initiation mechanisms [5] where explosive grains interact as multiple shock wave pass through damaged material. The binder is believed to have a strong effect on this mode of detonation as decohesion of the explosive grains from the binder allow the grains to interact directly under loads and provide an avenue for flame propagation. Thus, the fracturing behavior of propellants and high explosives are important to understanding XDT modes and the steps leading up to recompaction (such as inside rocket motor boreholes) requires an examination of the projectile impact response of energetic materials at the

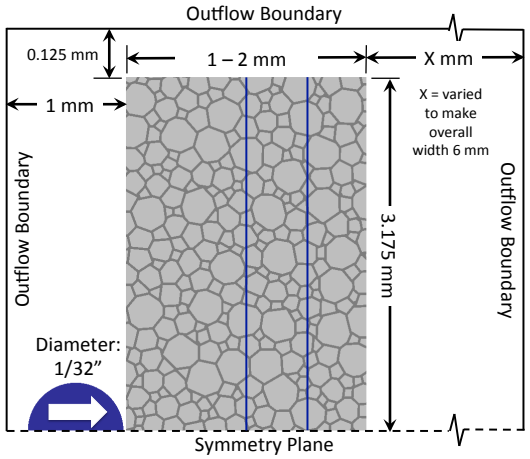

Fig. 1. Two-dimensional mesoscale simulation geometry

mesoscale.

In polymer binder systems the surface area of grains, binder strength, and adhesion of the binder to the grains will affect their response under impact loading conditions, thereby influencing the fracturing behavior. In studies carried out on PBX's, it was recognized that cracks formed preferentially at the interfaces of the binder with larger grains [6, 7, 8]. In our studies we choose to examine the effects of internal interfacial surface area by controlling the grain size and the transfer of stress and fragment generation by varying the strength of the polymer binder. More specifically we vary the grain size distribution of LX-10 HMX, near the main peak, to be 1.0, 0.50, or 0.25 times the original size. For the polymer binder strength, the binders are varied to have a range of properties such as the high ductility and low strength characteristics of HTPB to the more brittle and high strength behavior of epoxy.

While the polymer strength and grain size are important the volume fraction of the binder is also of interest. LX-04, for example, was found to have a lower degree of violence in Steven impact tests with increasing impact velocity [9] than other HMX-based explosives, which is thought to be due to the higher binder content (15 wt.%). In these experiments the authors noted that there was no evidence for a prompt detonation for these tests that typically have load durations of a few hundred microseconds. The reduced sensitivity to detonation with increasing violence in this material, based on our understanding, suggests that the increased binder content reduces either the generation of damage by reducing the amount of interfaces that act as decohesion sites or by increasing the materials inherent capability of transferring load throughout the microstructure and dissipating the intensity of the stress that causes damage. In mesoscale studies conducted on HMX/Estane binder formulations [10], the materials with a greater amount of binder was capable of dissipating work done by a shock front more easily. They also found the binder temperatures to be significantly lower for impacts at 500 m/s than at 1000 m/s. Since polymers are temperature and strain rate dependent, projectile impact velocity may play an important role. Therefore, in this study, the volume fraction of binder will be varied within the range of 75-95 vol.% to evaluate if similar effects modify the fracturing and damage behavior due to projectile impacts at velocities of 500 and 1000 m/s. To account for rate effects and strain localizations that occur within heterogenous microstructures, a rate dependent strength model is implemented.

Computational Approach

Simulation Setup

Two-dimensional plane strain mesoscale simulations of PBX's (HMX grains embedded in a polymer binder) were performed using ALE3D. The geometry of the simulation domain is shown in Figure 1 and consisted of a spherical aluminum projectile (1/32" diameter) impacting the cylindrical PBX pellets (3.175 mm diameter) at a normal incident angle and at velocities of 500 or 1000 m/s. A symmetry boundary was used along the pellet/projectile's axis of symmetry and outflow/inflow boundaries along the left, right, and top sides of the domain. Depending on the thickness of the pellet (1.0, 1.5, or 2.0 mm) the distance between the exit-side of the pellet and righthand side of the domain was varied so that the total domain width was 6mm. This was a balance between allowing the fragment cloud to develop and minimizing the overall computational costs. The zone size used in the calculations was 1-1.5 μm for a total of 8.8 - 19.8 million zones. This setup was chosen to not only be analogous to simplified ABVR tests (one-sided) but mimic new

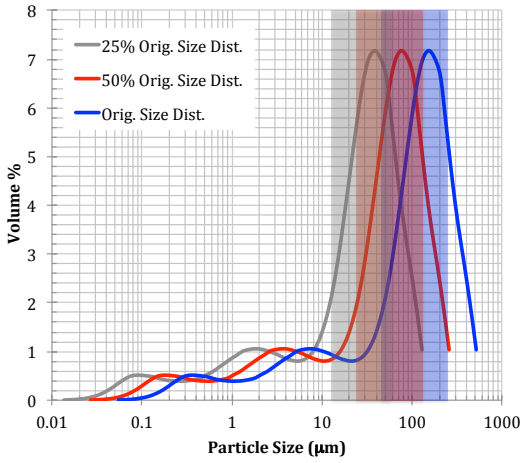

Fig. 2. Grain size distributions used for generating microstructures. Highlighted sections (same color as the line they correspond to) denote the grain sizes of interest for each distribution.

small-scale experimental capabilities currently being developed at LLNL.

Microstructure Generation

The grain size distribution for LX-10 was used as a reference point for producing simulated microstructures with varying grain size distributions (see blue line in Figure 2). The main LX-10 distribution peak is centered around $\sim$150 μm with a smaller peak centered at $\sim$7.5 μm. The majority of the LX-10 volume is comprised of this larger peak, as such we generated microstructures that had a baseline grain size distributions within the range of 48-240 μm using four bins (highlighted blue rectangle in Figure 2). The original distribution was truncated to this range to allow for the grain size to be varied to smaller sizes more readily without having to dramatically increase the mesh resolution of simulations and to eliminate large grain sizes that would potentially take up the majority of the simulated microstructure volume. We then varied the truncated grain size distribution to be .25x and .50x the original size. These shifted grain size distributions, as well as the 4-bin histogram data to generate the microstructures, are shown/listed in Figure 2 and Table 1 respectively.

The 4-bin grain size distributions were then used

Table 1. Histogram bin volume fractions and grain diameters used to capture the targeted section of the overall grain size distribution for each fractional size (25%, 50%, or 100% of the original distribution).

Bin (No.)	Bin V_f (–)	Orig. Dia. (μm)	0.50x Dia. (μm)	0.25x Dia. (μm)
1	0.08	240	120	60
2	0.26	144	72	36
3	0.41	80	40	20
4	0.25	48	24	12

in ParticlePack [11] to generate synthetic microstructures with varying solids (grain) loading that ranged from 45-95%. To generate the grains within a binder matrix, ParticlePack first constructs the randomly distributed grains and then recedes the interfacial boundaries back towards the adjacent grains using a distance specified by the user. By controlling the recession distance and each bin's grain size, specific microstructure compositions can be targeted. Although grain volume fractions ranged from 55-95 vol.% data will be shown for only a subset of those generated in this report. Figure 3 shows three representative microstructures that are 1.0 x 3.175 mm^2 in size – each with a different grain size distribution.

Material Model Parameters

The binder's constitutive behavior was modeled using a Steinberg-Guinan [12] type hardening model where the flow stress is modified by the plastic strain ($\overline{\varepsilon_p}$), and strain-rate ($\dot{\overline{\varepsilon_p}}$) according to the following equation:

$$Y_0 f\left(\overline{\varepsilon_p}, \dot{\overline{\varepsilon_p}}\right) = Y_0 \left[1 + \beta\left(\overline{\varepsilon_p} + \varepsilon_0\right)\right]^n \left[a + b\dot{\overline{\varepsilon_p}}\right]^m \quad (1)$$

where Y_0 is the initial yield strength, n and m the work hardening and rate senstivity exponents respectively, β the work hardening parameter, a an additive rate constant, b a strain rate normalization constant, and ε_0 a plastic strain offset. For the strain softening polymers, Kel-F and epoxy, Y_0 and the first bracketed section of Equation (1) is replaced with tabulated stress-strain data at a reference strain-rate. For Kel-F and Epoxy this refer-

Table 2. Strength and failure model parameter values for polymer binders

Polymer Binder	a (–)	b (/s)	m (–)	Y_0 (Mbar)	β (–)	ε_0 (–)	n (–)	σ_f (Mbar)	ε_f (–)
Kel-F	0.001	1.9e4	0.15	–	–	–	–	-1.0e-3	1.0
HTPB	0.25	250.0	0.25	8.5e-6	0.5	0.025	0.5	-0.2e-3	3.0
Epoxy	0.085	249.0	0.14	–	–	–	–	-2.0e-3	0.5
PTFE	1.0	250.0	0.15	1.3e-4	1.7	0.05	1.75	-2.0e-3	1.5

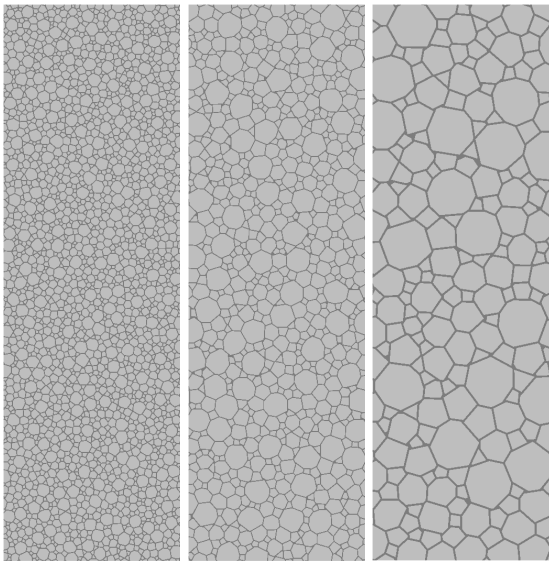

Fig. 3. Representative microstructures (1.0 x 3.175 mm^2) used in calculations. From left to right the volume fraction of grains are 75%, 85%, and 85% with grain size distributions of 25%, 50%, and 100% the original distribution respectively. While they appear somewhat circular in the figure, the grains are blocky in nature at higher magnification.

ence strain-rate is 100 s^{-1} and 1300 s^{-1} respectively. The strength parameters for different polymer binders are given in Table 2. A stress (σ_f) and strain (ε_f) criteria for failure is implemented, and the parameters are also included in Table 2. A stress strain curves for Kel-F and PTFE are shown in Figure 4 to give an idea of the relative fit of model parameters to experimental data each formulation of Equation (1).

A seven-term polynomial was used to model the binder's equation-of-state (EOS) in which the pressure is related to the compression (μ) and internal energy (E) of the material through the relation:

$$P = a_0 + a_1\mu + a_2\mu^2 + a_3\mu^3 + \left(b_0 + b_1\mu + b_2\mu^2\right) E \quad (2)$$

where a_0 is a pressure constant, a_1, a_2, and a_3 are bulk moduli coefficients, b_0 the Grüneisen coefficient, and b_1 and b_2 corrections to the Grüneisen coefficient. In our studies a_0, b_1, and b_2 were all set to zero. Values for the remainder of the EOS model parameters are given in Table 3 for the polymer binders.

Table 3. Seven-Term Polynomial EOS model parameters for polymer binders. The parameters a_0, b_1, and b_2 were all set to zero.

Polymer Binder	a_1 (Mbar)	a_2 (Mbar)	a_3 (Mbar)	b_0 (–)
Kel-F	0.1	0.075	0.75	1.097
HTPB	0.029	0.0	1.25	1.45
Epoxy	0.10	0.05	0.50	0.80
PTFE	0.015	0.005	0.35	0.59

Results and Discussions

Grain Size Effects on HE Fragmentation

Figures 5 and 6 show the development of plastic strain within the binder material for different grain size distributions as well as a comparison of the plastic strain histograms for microstructures composed of 85% grain volume fraction and Kel-F binder. Microstructures containing the larger grain size distributions resulted in a more heterogenous pressure front, and produced more localized stress/strain bridging, which propagated throughout the microstructure more quickly than in microstructures with smaller grain sizes. In regions

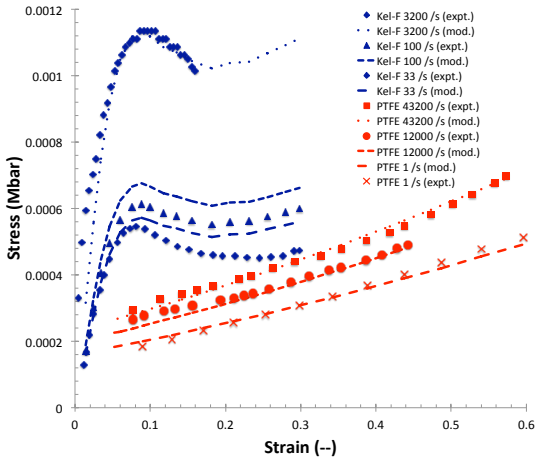

Fig. 4. Fit of the strain rate dependent model to experimental data for Kel-F[13, 14] (blue) and PTFE[15] (red), at various strain rates, using values in Table 2.

away from the impact site the stress/strain bridging appeared to be communicated along paths that connected the largest grains, which also provided some stress shielding for the smaller grains within the microstructure. For microstructures with larger grain sizes, we also found the zones within the binder directly adjacent to the grains strained more quickly than the interior region of the binder between grains. These effects are consistent with observations of cracks preferentially forming at the binder/grain interface of larger grains within the microstructure [6, 7, 8].

Apart from the region directly within the cross-sectional path of the projectile the corners (junctions) of multiple grains had the greatest strain values. From the histograms we found that at times less than 1 μs the extent of binder strain is fairly similar across the various grain sizes. However, at later times, greater than 1 μs, the straining increases with increasing grain size and is accompanied with not only higher max strains but broader strain distributions.

Effects of Binder Volume Fraction

With increasing amounts of binder, the HMX grains take up less of the load as the pressure waves move throughout the microstructure. This translates into the binder undergoing larger shear deformation and dissipating the load transferred to the HMX grains. The effect on the HMX grains was significant with much larger plastic strain accumulating in HMX grains for microstructures with less binder (see Figure 7). Additionally, strain bridging was found to be more pronounced in microstructures with a larger percentage of binder and still predominately followed paths connecting larger grains. This behavior is shown in Figure 8. We also observed the plastic strain distribution for the binder to broaden with decreasing binder content (see Figure 9).

Effects of Binder Strength

The binder's strength characteristics plays a key role in the deformation of polymer bonded explosive composites under high velocity impacts. For microstructures containing softer binders in relation to Kel-F, such as HTPB, had much lower strains in both the binder (see histogram in Figure 10) and HMX grains. The opposite is true of microstructures with stronger materials such as epoxy. When the Kel-F binder was replaced with epoxy, the strains within the HMX grains increased and the binder plastic strain histograms broadened significantly. The propagation of failure of the binder occurred more rapidly in these instances, which results in the generation of more fragments.

Velocity Effects

Not surprisingly, a decrease in velocity from 1000 m/s to 500 m/s resulted in smaller strains, and more narrow histogram distribution, for a given time. However, the difference was in general fairly small and may be indicative of a greater dependence on binder strength and microstructure than impact velocity once the stress magnitudes reach a certain level. At impact velocities of 500 m/s the aluminum projectile had very limited deformation, where as impacts at 1000 m/s the projectile had undergone more significant deformation. In experiments we have found 500 m/s to be sufficient for the aluminum projectile to penetrate through LX-10 samples of similar size with little or no noticeable deformation. No experiments have been conducted at lower/higher impact velocities however, and therefore a threshold velocity for penetration in theses

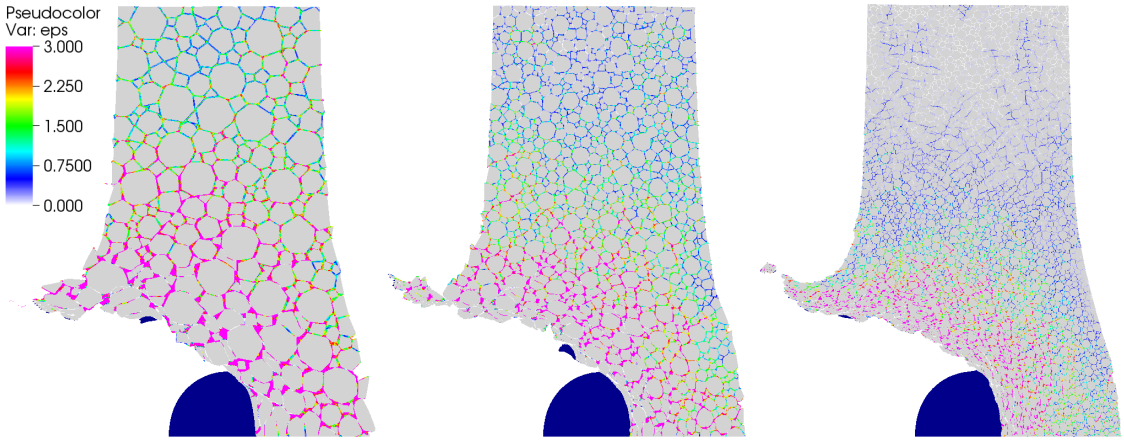

Fig. 5. Plastic strain within the Kel-F binder after 2 μs following an impact of an aluminum sphere at 1000 m/s. The grain volume fraction is 85% and grain size distributions are 100%, 50%, and 25% (from left to right) the original distribution grain size.

types of formulations has yet to be resolved.

Conclusions and Future Studies

Based on these simulations, the following generalized trends were observed. Firstly, increasing amounts of binder decreased the accumulation of strain in the HMX and translated into more work being done on the binder. In delayed XDT reactions that involve these types of formulations, onset of ignition may be a limited to conduction of heat from the binder to the HMX grains.

Second, larger grain size distributions result in more deformation of both the HMX and binder, with more straining occurring along percolation paths containing larger grains. This results in more damage/fragmentation across the entire sample at earlier times thereby increasing chances for ignition due to friction from interactions between grains or secondary impacts of fragments against surfaces downstream from the sample (such as against rigid surfaces or in BVR tests with two slabs of propellant, which are analogous to rocket motor bores).

Thirdly, microstructures with HTPB had less plastic straining of both the binder and HMX grains, where as those with epoxy had increased straining in both the HMX and binder. This results in the generation of fewer (larger) fragments or more (smaller) fragments for formulations with weaker/stronger binders respectively. In ABVR tests with smaller gap distances, there is often less of a chance for XDT reactions to take place since the fragment cloud doesn't have a chance to rarify be recompacting. For formulations of propellants or high explosives that may contain stronger binders smaller gap distances may be needed to reduce chances of XDT reaction upon recompaction.

In our simulations inference of fragment production came from the deformation of the individual constituents at fairly early times. Future simulations will address the incorporation of more advanced failure models that are more representative of physical observations. They will also include an anvil, with varying strength, on the downstream side of the fragment cloud to investigate the contributions of secondary impacts and recompaction (between the projectile and anvil) to XDT modes or reaction, such as those observed for propellants inside rocket bores. Temperature distributions within the fragments upon striking these anvils will be monitored. Other topics of interest are the effects of porosity on the fragmentation of PBX's under these high velocity impacts and the projectile's geometry and size. Since fracturing of materials has three-dimensional attributes, such as the stress bridging of grains, simulations will also be conducted on three-dimensional microstructures generated in the same manner. Obtaining a threshold velocity for penetration is also of interest and is important for compari-

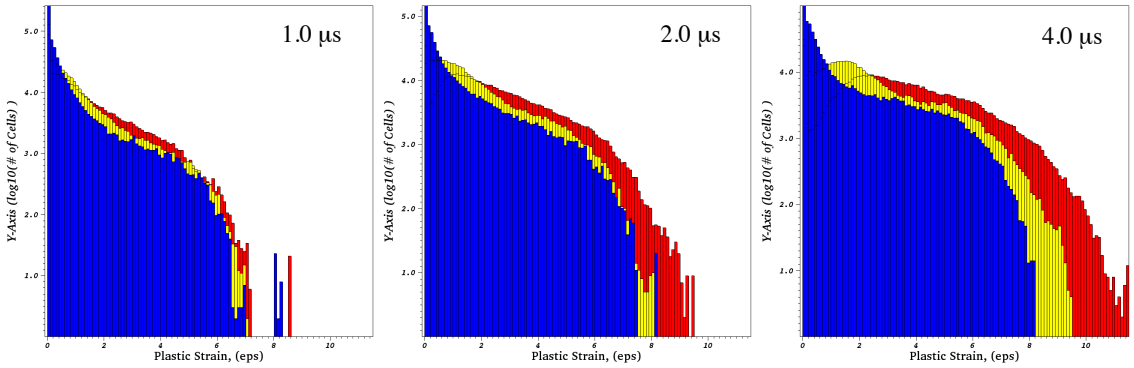

Fig. 6. Plastic strain histograms for Kel-F after 1 to 4 μs following an impact of an aluminum sphere at 1000 m/s. The grain volume fraction is 85% and grain size distributions of 100% (red), 50% (yellow), and 25% (blue) the original LX-10 HMX grain size distribution.

son of models to experimental data.

Acknowledgements

This work was performed under the auspices of the U.S. Department of Energy by Lawrence Livermore National Laboratory under Contract DE-AC52-07NA27344. This work was supported by the Joint DoD-DOE Munitions Technology Development Program. LLNL Technical Report, LLNL-PROC-656539.

References

1. Nichols III, A. L., "ALE3D User's Manual, Version 4.22," *Technical Report LLNL-SM-650174*, Lawrence Livermore National Laboratory, January 2014.

2. Schmitt, R. G., Taylor, P. A. and Hertel, E. S., "Application of a Multiphase Mixture Theory with Coupled Damage and Reaction to Energetic Material Response," in "Proceedings of the 12th International Detonation Symposium, San Diego, California, August 11-16, 2002," 1, pp. 475–482, 2002.

3. Finnegan, S., Pringle, J., Schulz, J. and Alexander, M., "A planar rocket motor model for visualization of violent reaction due to fragment impact," *Technical Report NWC-TP-7074*, Naval Weapons Center, China Lake, CA, 1990.

4. Matheson, E. R. and Rosenberg, J. T., "A Mechanistic Study of Delayed Detonation in Impact Damaged Solid Rocket Propellant," in "Proceedings of the Conference of the American Physical Society Topical Group on Shock Compression of Condensed Matter," Vol. 620, pp. 464–467, AIP Publishing, 2002.

5. Matheson, E. R. and Rosenberg, J. T., "The Role of Damage Mode in Delayed Detonation of Composite Energetic Materials," in "Proceedings of the 12th International Detonation Symposium, San Diego, California, August 11-16, 2002," 1, pp. 451–458, 2002.

6. Rae, P., Palmer, S., Goldrein, H., Field, J. and Lewis, A., "Quasi–static studies of the deformation and failure of PBX 9501," *Proceedings of the Royal Society of London. Series A: Mathematical, Physical and Engineering Sciences*, Vol. 458, pp. 2227–2242, 2002.

7. Rae, P., Goldrein, H., Palmer, S., Field, J. and Lewis, A., "Studies of the failure mechanisms of polymer bonded explosives by high resolution moiré interferometry and environmental scanning electron microscopy," in "11th Detonation Symposium, Snowmass C," p. 31, 1998.

8. Chen, P., Huang, F. and Ding, Y., "Microstructure, deformation and failure of polymer bonded explosives," *Journal of materials science*, Vol. 42, pp. 5272–5280, 2007.

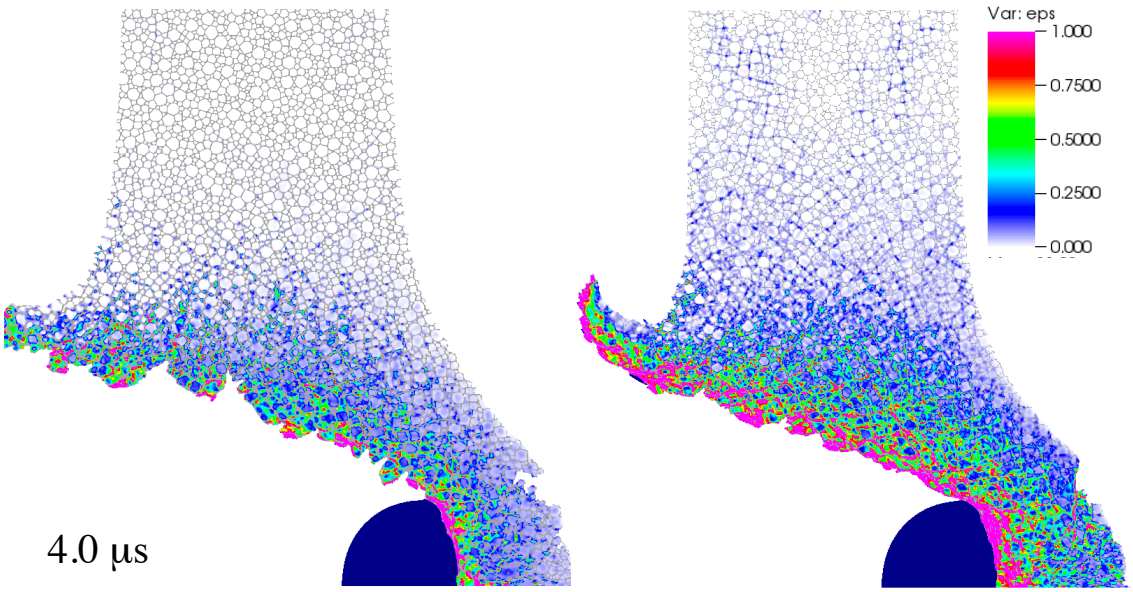

Fig. 7. Plastic strain accumulation within HMX grains for microstructures containing binder volume fractions of 25% (left) and 15% (right). Grain size distribution of 0.25x.

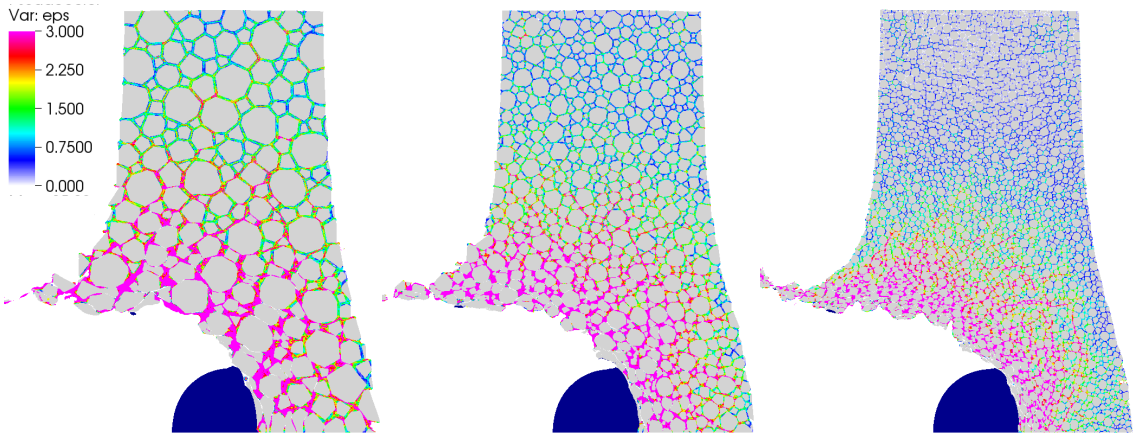

Fig. 8. Plastic strain within the Kel-F binder after 2 μs following an impact of an aluminum sphere at 1000 m/s. The grain volume fraction is 75% and grain size distributions are 100%, 50%, and 25% (from left to right) the original distribution grain size.

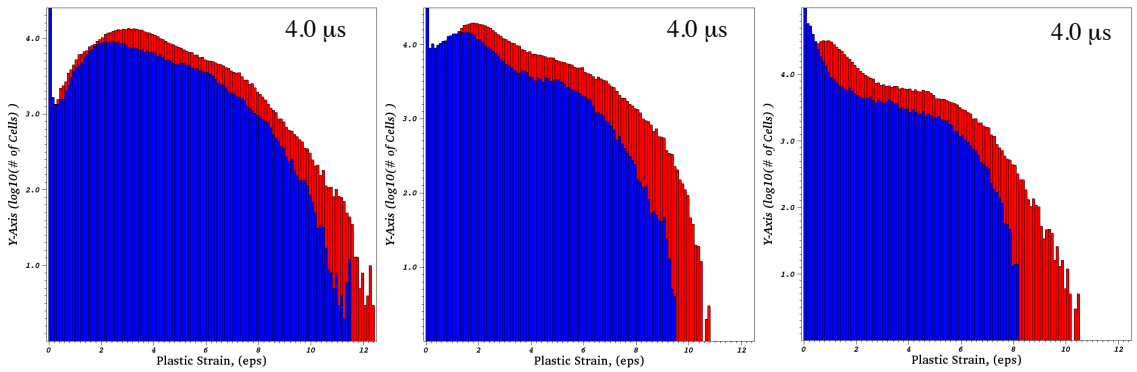

Fig. 9. Plastic strain histograms for Kel-F after 1 to 4 μs following an impact of an aluminum sphere at 1000 m/s. The grain volume fractions are 85% (blue) and 75% (red) for grain sizes of 100%, 50%, and 25% the original LX-10 HMX grain size distribution left to right respectively.

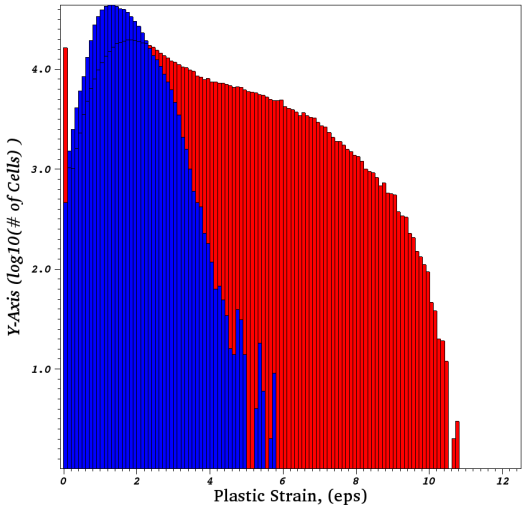

Fig. 10. Plastic strain histograms for Kel-F (red) and HTPB (blue) 4 μs following an impact of an aluminum sphere at 1000 m/s. The grain volume fraction is 75% (blue) and the grain sizes 50% the original LX-10 HMX grain size distribution.

9. Chidester, S. K., Vandersall, K. S., Switzer, L. L. and Tarver, C. M., "LX-04 Violence Measurements-Steven Tests Impacted by Projectiles Shot from a Howitzer Gun," in "AIP Conference Proceedings," Vol. 845, p. 1049, IOP Institute of Physics Publishing LTD, 2006.

10. Conley, P., Benson, D. and Howe, P. M., "Microstructural effects in shock initiation," in "Proceedings of the 11th International Detonation Symposium, Snowmass, Colorado," 1, pp. 768–780, 1998.

11. Friedman, G., "ParticlePack User's Manual, Version 3.0," *Technical Report LLNL-SM-649196*, Lawrence Livermore National Laboratory, December 2013.

12. Steinberg, D. J., "Equation of State and Strength Properties of Selected Materials," *Technical Report UCRL-MA-106439*, Lawrence Livermore National Laboratory, February 1991.

13. Brown, E. N., Rae, P. J. and Gray III, G. T., "Compressive properties of four fluoropolymers as a function of temperature and strain rate," in "Proceedings of the 2007 SEM Annual Conference Exposition on Experimental and Applied Mechanics," 2007.

14. Clements, B. E., Mariucescu, L., Brown, E. N., Rae, P. J., Orler, E. B., Dattelbaum, D. M., Sheffield, S. A., Robbins, D. L., L., G. R. and Velisavlijevic, N., "Kel-F 800 Experimental Characterization and Model Development," *Technical Report LA-UR-07-6404*, Los Alamos National Laboratory, 2007.

15. Jordan, J. L., Siviour, C. R., Foley, J. R. and Brown, E. N., "Compressive properties of extruded polytetrafluoroethylene," *Polymer*, Vol. 48, pp. 4184–4195, 2007.

Comments

A. Kuhl, LLNL

The Steinberg-Guinan Model gives a pressure and sound speed for all volumes. But after the material goes into tension, the stress and sound speed go to zero. Thus the constitutive relations seem to be in error for the materials in tension. Then one needs to treat the particles as discrete Lagrangian particles (rather than a continuum).

Reply by B. White, LLNL

There are certainly a variety of numerical approaches that may be used to model fragmentation, with each having their own deficiencies. While the binder constitutive behavior was based on the Steinberg-Guinan (S-G) model, it was not implemented explicitly. We also used a different equation of state than what is typically used with the S-G model and a failure criteria based on stress and strain. We intend on exploring other means of handling the fracture behavior of PBX's at the mesoscale.